REDUCTION MECHANISM OF TITANOMAGNETITE CONCENTRATE BY CARBON MONOXIDE
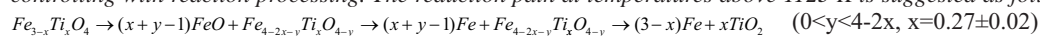
X.F. She[a,b], H.Y. Sun[a,c], X.J. Dong[a], Q.G. Xue[a], J.S. Wang[a,*]

[a] State Key Laboratory of Advanced Metallurgy, School of Metallurgical and Ecological Engineering, University of Science and Technology Beijing, Beijing, P.R. China
[b] School of Mechanical Engineering, University of Science and Technology Beijing, Beijing, P.R. China
[c] State Key Laboratory of Multiphase Complex Systems, Institute of Process Engineering, Chinese Academy of Sciences, Beijing, P.R. China

Abstract

Titanomagnetite concentrate was reduced by CO-Ar gas mixtures in a laboratory fixed bed reactor in the temperature range from 1123 to 1323 K. The influences of reductive conditions on the reduction rate and metallization degree including reduction temperature, reduction time and carbon monoxide content were studied. And the characteristics of reduced samples were analyzed by XRD, BES and EDS. Results shown that both the reduction and metallization degree increased with the increasing of temperature and monoxide content. The low reduction degree was owing to the low iron oxides content and high impurities content such as magnesium oxide in titanomagnetite concentrate. Above 1123 K, the reduction is controlled by interfacial chemical reaction at early stage of the reaction and then turns to the internal diffusion controlling with reaction processing. The reduction path at temperatures above 1123 K is suggested as follow:

$$Fe_{3-x}Ti_xO_4 \rightarrow (x+y-1)FeO + Fe_{4-2x-y}Ti_xO_{4-y} \rightarrow (x+y-1)Fe + Fe_{4-2x-y}Ti_xO_{4-y} \rightarrow (3-x)Fe + xTiO_2 \quad (0<y<4-2x, x=0.27\pm0.02)$$

Keywords: Titanomagnetite concentrate; Reduction; Carbon monoxide; Reduction path; Reduction kinetics.

1. Introduction

The demand for titanium dioxides which are widely used in paint, paper and plastics industries is increasing rapidly [1]. At present, ilmenite (40-65% TiO_2) is the main sources for production of metallic titanium and titanium containing compounds [2]. Since the sources of high-grade titania-ferrous ores are decreasing in the world, the utilization of low-grade minerals such as titanomagnetite (TTM, 10-16% TiO_2) has attracted more attention [3, 4]. China has the largest titania-ferrous ores reserve about $2x10^8$ t (in TiO_2) [5]. Panzhihua titanomagnetite accounts for more than 90% titanium reserves in China and more than 35% around the world [6]. At present the TTM concentrate is mainly smelted in the blast furnace (BF) to make iron and most of titanium components in the ore are concentrated into molten slag (22-25% TiO_2) [7]. Due to the scattered distribution of titanium components in various fine grained mineral phases (<10 μm) with complex interfacial combination, it is difficult to recover the titanium components and metallic iron through traditional separation processes [8].

In the past decades, a number of researches have been conducted to improve the utilization of titania-ferrous ores, including smelting [9], direct acid leaching [10], selective chlorination [11] and reduction [12]. Among these, the direct reduced iron (DRI) process is supposed to be a more practical and effective way. In the industrial production, DRI - electric arc furnace (EAF) melting separation method has been proposed for refining both iron and Ti slag from the TTM concentrate. In this method, the role of DRI process is to produce pre-reduction pellets (with the metallization degree 60-75%) for EAF melting and reduction equipment mainly uses the rotary-kiln [3]. However, the solid state carbothermic reduction in rotary-kiln is relatively slow with high-energy consumption and narrow range of operating temperature [13,14], which stimulates researches into gaseous reduction of titania-ferrous ores. Vijay investigated the reduction of Quilon ilmenite beach sand with hydrogen in a fluidized bed reactor and found the reduction period could be divided into three distinct stages: initial slow induction stage, intermediate acceleratory stage and final slowing down stage[15]. The results of Park's work shown that the reduction of New Zealand TTM ironsand in the fixed bed reactor by carbon monoxide gas was slower

---

than that of hematite or magnetite iron ores [16]. Wang studied the hydrogen reduction kinetics of Bama ilmenite and considered that diffusion of hydrogen gas in the reduced layer was the rate controlling step [17].

Although the reduction of titania-ferrous ores by gas mixtures has been studied intensively by some research groups, the information on the reduction of TTM concentrate by carbon monoxide is still few, especially in the kinetics and the phase transformation during the reduction. And because carbon monoxide is a major reducing agent in DRI processes with hydrogen, it is necessary to clarify the mechanism of the reduction of TTM concentrate by carbon monoxide for the future application. The aim of this work is to investigate the isothermal reduction behaviors of TTM concentrate by carbon monoxide. The influences of reductive conditions on the reduction rate and metallization degree of TTM concentrate such as reduction temperature, reduction time and carbon monoxide content were studied. Also the characteristics of reduced samples, reduction path and reductive kinetics were analyzed.

2 Experimental
2.1. Materials

The TTM concentrate used in this study was obtained from Panzhihua, in Sichuan province of China. After drying and grinding, the particle size of concentrate was 5.03-64.79 μm. Chemical composition of concentrate is listed in Table 1. Phase characteristic of sample was investigated by XRD. The result in Fig. 1 indicates that the main crystalline phases of concentrate are TTM ($Fe_{3-x}Ti_xO_4$, with x=0.27±0.02, or $3(Fe_3O_4)\cdot Fe_2TiO_4$) and few ilmenite

($FeTiO_3$ or $FeO\cdot TiO_2$).

2.2. Experimental procedures

The concentrate was pressed in a closed die of 9 mm in diameter under 15 MPa to produce cylindrical pellets with mass of about 2 g and height of 8 mm. The reduction of TTM concentrate using CO-Ar gas mixture was studied in a laboratory fixed bed reactor equipment as presented in Fig. 2. Before starting each experiment, the reactor system with sample in it was first purged by argon gas at room temperature to reduce the concentration of oxygen in the reactor. Then the sample was heated to the experimental temperature in argon atmosphere and the reduction started by introducing CO-Ar gas mixture to the reactor. After a certain reaction time, the sample was pulled off from the reactor and quenched. The carbon monoxide and argon gas used in the experiments were super high purity and high purity, respectively. The gases were purified before mixing by passing through traps filled with drierite and a molecular sieve to remove moisture. The composition of reducing gas was achieved using gas flow controllers (Brooks, Model 5850E). The total reducing gas flow rate was maintained at 2 L/min, which was sufficient to neglect the external mass transfer resistance in the gas phase.

During the experimental process, the weight changes of reacting samples were monitored by electronic balance (Mettler-Toledo AL104) and recorded in real-time by computer. The mineralogical
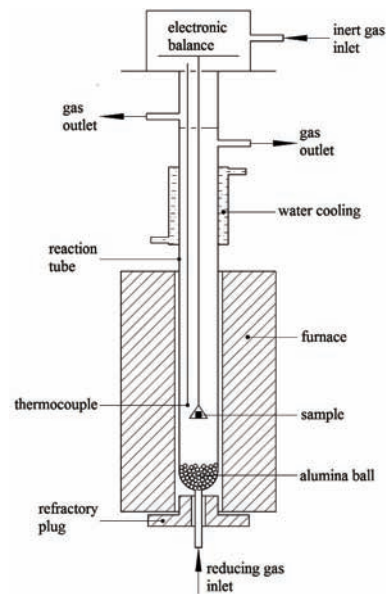

Figure 1. XRD pattern of titanomagnetite concentrate

Figure 2. Schematic diagram of the apparatus

Table 1. Chemical composition of titanomagnetite concentrate (wt.%)

TFe	FeO	Fe_2O_3	TiO_2	SiO_2	MgO	Al_2O_3	V_2O_5	CaO	MnO
54.54	32.16	42.18	10.77	3.81	3.72	3.54	0.67	0.39	0.4

morphology of sample was examined by XRD (Nikkaku D/max-RB, using Cu Kα), BES (JSM-6480LV) and EDS (Noran System six).

3. Results and discussion

In the previous work analysis [18], an almost direct correlation between total mass loss and oxygen loss can be assumed since the analysis of the outlet gas during the reduction showed it to consist of CO_2. Therefore the experimental results were presented in terms of the ratio of mass loss against reduction time. The reduction degree (w) is defined as

$$w = \frac{w_0 - w_m}{w_t} \times 100\% \qquad ...(1)$$

where w_0 is the starting mass of sample after removal of moisture, w_m is the mass of sample after reduction time t, and w_t is the total possible mass loss for the reduction of TTM concentrate corresponding the weight of oxygen in Fe_2O_3 and FeO. The metallization degree (η) of each sample was calculated by following formula:

$$\eta = (MFe/TFe) \times 100\% \qquad ...(2)$$

where MFe is the weight of metallic iron after reduction, TFe is the weight of total iron after reduction. The total iron content was analyzed by ICP-AES and metallic iron was analyzed by chemical method. The porous samples after reduction were analyzed and the reductive kinetics were discussed in detail as follows.

3.1 Effect of temperature

Plots of the reduction and metallization degree of TTM concentrate reduction by 50 vol% CO-Ar gas mixtures as a function of time are shown in Figs. 3 and 5. From figures, it can be seen that temperature influences the reduction and metallization degree. With temperature increasing, both the reduction and metallization degree increase. Compared with the experimental results of Park [16], the reduction degree of TTM concentrate from Panzhihua is lower than that of TTM ironsand from New Zealand, which could be attributed to the fact that TTM concentrate examined in the present experiments is composed of lower content of iron oxide and higher content of iron titanium oxide and impurities such as magnesium oxides. But even reduced for 120 min at 1323 K, iron oxides in TTM concentrate from Panzhihua are still not entirely reduced. On one side, it was established that the gaseous reduction of TTM is much slower than that of hematite and magnetite iron ores[19,20]. The complete reduction of iron oxides in TTM by carbon monoxide requires temperature above 1273 K and high reducing potential[21]. On the other side, the impurities oxides in TTM could impede reduction, which can be explained by the barrier

effect as follws [22]. It is known from thermodynamic calculation that during the reduction of TTM concentrate, it is neither possible to reduce magnesium oxide in the TTM to magnesium metal nor could magnesium pass into solid solution in titanium oxide [23]. During the reduction of TTM concentrate, the magnesium concentration ahead of the reduction interface increased in TTM concentrate by direct reduction of Fe^{2+}. This lowered the thermodynamic activity of the Fe^{2+}, making its reduction progressively more difficult. Eventually, the magnesium concentration became so high, and the iron activity was so low that the reduction of Fe^{2+} to metallic iron almost stopped. Similarly, manganese and aluminum oxides have the same effect on the reduction kinetics as magnesium oxide since the impurities oxide content of the briquette increases the barrier effect [24, 25]. However, magnesium oxide has somewhat larger effect on the reduction kinetics than manganese oxide. This might be due to the fact that magnesium oxide forms a more stable solid solution with titanium and iron oxides than other impurities oxides.
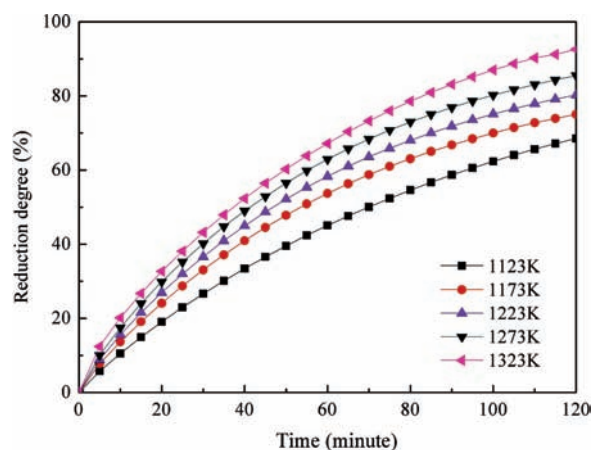

Figure 3. *Reduction of titanomagnetite concentrate by 50 vol% CO-Ar mixtures at various temperatures*

3.2 Effect of carbon monoxide content

Effect of carbon monoxide content on the reduction of TTM concentrate was studied at 1173 K. The carbon monoxide content was varied from 15 to 100 vol%. The reduction curves are presented in Fig. 4. As shown in Fig. 4, the increase of carbon monoxide content from 15 to 100 vol% caused an obvious increase in the reduction degree. And with 100 vol% CO gas, the fractional weight loss was found to reach a maximum at some later stage of reduction and then the pellet appeared to gain weight, this is because the rate of carbon deposition exceeded that of the reduction process with the condition of high metallization degree and carbon monoxide content [26, 27].
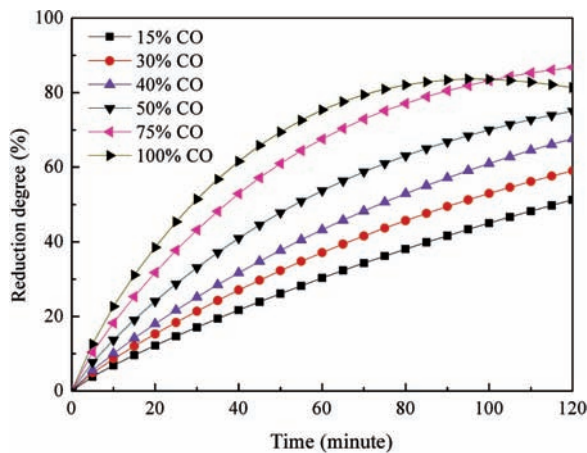
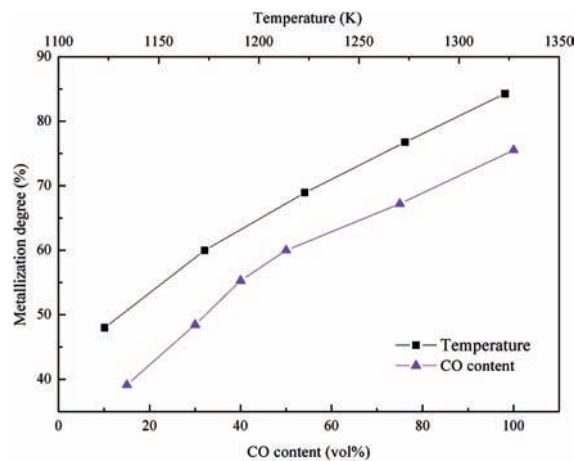**Figure 4.** *Reduction of titanomagnetite concentrate by CO-Ar mixtures with different CO content at 1173 K*

Figure 5. *Effect of temperature and CO content on the reduction of titanomagnetite concentrate*

3.3 Phase transformation during reduction of titanomagnetite concentrate

In the experimental condition, the reduction temperature affected the reduction and metallization degree as well as the composition of sample significantly. Fig. 6 presents the final reduction products at different temperature after 120 min reaction. At 1123 K and 1173 K, when the metallization degrees are 47.98% and 59.77%, respectively, wüstite peaks as a transition phase are detected. Although there are some ilmenite contained in the raw ore of TTM concentrate, ilmenite also can be considered as a produced phase in the progress of reduction with higher peaks. Starting from 1223 K, wüstite disappears in the sample with the metallization degree 68.91%. At higher temperature 1223-1323 K, no new phase appeared, but both the peaks of TTM and of ilmenite become weaker at 1323 K with the metallization degree 84.26% than those at 1223 K, indicating that ilmenite also is a transition

phase. Even after 120 min reduction at 1323 K, the peaks of Ti oxides are still not detected. This may be due to the low Ti oxides content, and further investigation such as TEM and MLA observation can be used for clarifying the formation of TiO_2[28].
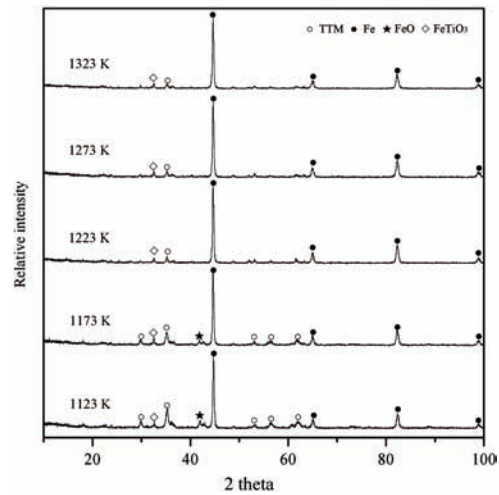

Figure 6. *XRD patterns of samples reduced by 50 vol% CO-Ar mixtures at various temperatures for 120 min*

Samples in the process of reduction at 1173 K were analyzed by XRD as shown in Fig. 7. With 15 min reduction, there are mainly four phases in the samples, TTM, wüstite, metallic iron and ilmenite phases. The metallization degree of samples reduced for 15, 30, 45, 60 and 90 min are 14.03%, 25.86%, 37.79%, 45.30% and 56.58%, respectively. With reduction time and metallization degree increasing, the peaks of TTM, wüstite and ilmenite phases become weaker and those of metallic iron get stronger. Particularly, although wüstite and ilmenite phases are not disappeared, their peaks as transition phases are obviously getting weak with reduction
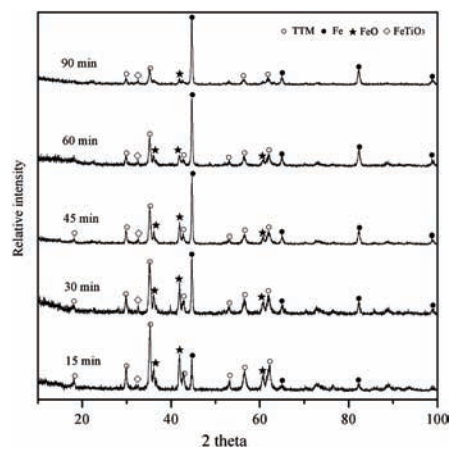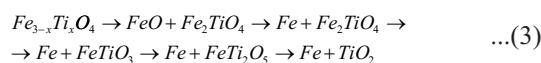

Figure 7. *XRD patterns of samples reduced by 50 vol% CO-Ar mixtures at 1173 K in the progress of reduction*

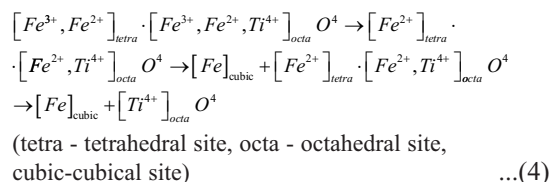processing, which is consistent with analysis from Fig. 6.

According to the previous studies about the phase relations and the equilibrium oxygen partial pressures in the Fe-Ti-O ternary system in the temperature range of 1173-1373 K, which employed the CO-CO_2 circulation method, the reduction of TTM in the Fe-Ti-O system would proceed the following path [29, 30]:
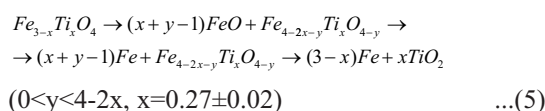
$$Fe_{3-x}Ti_xO_4 \rightarrow FeO + Fe_2TiO_4 \rightarrow Fe + Fe_2TiO_4 \rightarrow$$
$$\rightarrow Fe + FeTiO_3 \rightarrow Fe + FeTi_2O_5 \rightarrow Fe + TiO_2 \qquad ...(3)$$

The reduction path includes the formation of intermediate Ti-containing phases such as ülvospinel (Fe_2TiO_4), ilmenite ($FeTiO_3$) and ferrous-pseudobrookite ($FeTi_2O_5$). In the equilibrium state, the transformation in structure of Ti-containing phase during the reduction of TTM concentrate can be presented by the following sequence:

TTM (spinel cubic)→ülvospinel (spinel cubic)→ilmenite (rhombohedral)→ferrous-pseudobrookite (orthorhombic)→rutile

The first step includes the transformation of TTM to wüstite and ülvospinel with the rearrangements of Fe^{2+} in tetrahedral and octahedral sites in the lattice, and then it is the transformations from Fe^{2+} in tetrahedral and octahedral sites to the cubic metallic iron as shown in Eq.(4) (The structure of TTM was presented by the Akimoto model [28, 31]).

$$\left[Fe^{3+}, Fe^{2+}\right]_{tetra} \cdot \left[Fe^{3+}, Fe^{2+}, Ti^{4+}\right]_{octa} O^4 \rightarrow \left[Fe^{2+}\right]_{tetra} \cdot$$
$$\cdot \left[Fe^{2+}, Ti^{4+}\right]_{octa} O^4 \rightarrow \left[Fe\right]_{cubic} + \left[Fe^{2+}\right]_{tetra} \cdot \left[Fe^{2+}, Ti^{4+}\right]_{octa} O^4$$
$$\rightarrow \left[Fe\right]_{cubic} + \left[Ti^{4+}\right]_{octa} O^4$$

(tetra - tetrahedral site, octa - octahedral site, cubic-cubical site)   ...(4)

In experiments, XRD results (Figs. 6 and 7) showed that the fast step in the reduction is TTM to wüstite starting with the reduction of Fe^{3+} to Fe^{2+} and wüstite to Fe accompanied by the removal of oxygen. Titanium in TTM stabilizes the spinel structure, so the slow step in the reduction is the release of Fe^{2+} from the titania-ferrous phase (that is, from ilmenite and ferrous-pseudobrookite to metallic iron). Based on the above analysis, the reduction path of TTM under the experimental condition is presented as follow:

$$Fe_{3-x}Ti_xO_4 \rightarrow (x+y-1)FeO + Fe_{4-2x-y}Ti_xO_{4-y} \rightarrow$$
$$\rightarrow (x+y-1)Fe + Fe_{4-2x-y}Ti_xO_{4-y} \rightarrow (3-x)Fe + xTiO_2$$

(0<y<4-2x, x=0.27±0.02)   ...(5)

3.4 Morphology and energy disperse spectroscopy analysis

Morphology of particles in the progress of TTM concentrate reduction by 50 vol% CO-Ar mixture at 1173 K were examined by BES (Fig. 8). It can be seen
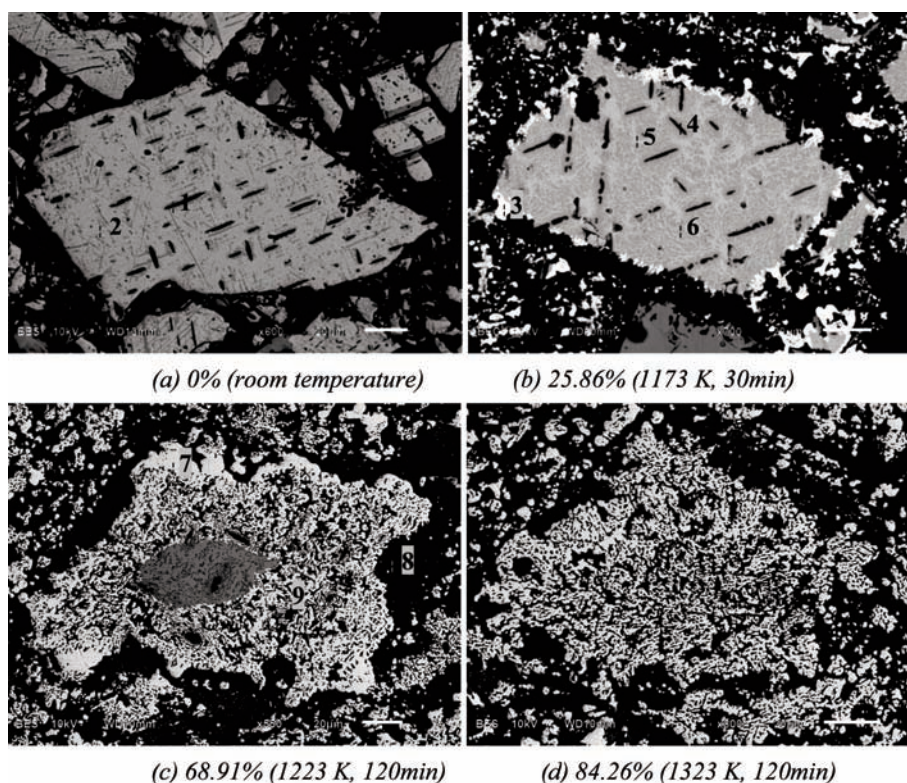

(a) 0% (room temperature)   (b) 25.86% (1173 K, 30min)

(c) 68.91% (1223 K, 120min)   (d) 84.26% (1323 K, 120min)

Figure 8. *Morphology changes of titanomagnetite concentrate particles during the reduction by 50 vol% CO-Ar mixtures (in the order of metallization degree, %)*

from Fig. 8(a) that the raw ore of TTM concentrate consists of non-homogeneous particles with impurities oxides phase having a lamella structure. According to EDS analysis (Table 2), the black impurities oxide region with an atom ratio [Al]/[Mg]=2.62 is mainly consist of magnesia-alumina spinel (MgAl$_2$O$_4$, with an atom ratio [Al]/[Mg]=2) with high Al content, and the white background is TTM. As reduction progressing, the reduced iron first appears at outside surface of particle and the phase at the inner of particle is basic invariable (Fig. 8(b)). In general, four different morphological regions are identified in the reacted pellets. White region is the reduced iron phase. Dark gray region is the unreacted magnesia-alumina spinel phase. And the rearrangement TTM substrate contains two regions, the light gray and gray regions. The light gray region rich in iron is the preferential reduction zone for iron oxide. The gray region concentrating much Ti oxide can be regarded as the slag forming region. Although the light gray region has lower content of impurities oxides than the gray region, the content of Mg as a more stable barrier impurity is still higher than it in the gray region, which is consistent with the previous analysis about the effect of impurities on reduction rate. Overall, the reduction of the TTM concentrate particles started in a topochemical way with the formation of reduced/unreduced interface and this is more evident on Fig. 8(c). From Fig. 8(c), it can be seen that the product layer is a rough and porous structure, and the reduced iron phase accumulates on the reticular slag phase. Actually, by morphology and elemental composition analysis (Table 2), the reticular slag is not the reduced product but the in-situ residual slag due to the microscopic non-homogeneity of TTM particle. However, the slag distributing in the reduced iron is the reduced product. With reduction progressing, the area of unreduced core is getting smaller and disappeared at last (Fig. 8(d)). But even at the end of the reaction, the reduced iron or slag is still not connected together to form a uniform continuous area. This is because the low reduction temperature and the high melting point of Ti-containing slag [32].

3.5 Reaction kinetics

Based on the observed results, it can be concluded that the reduction of the pellet proceeded topochemically. According to previous studies [33, 34], this kind of reaction includes the process of diffusion of gaseous species and that of intrinsic chemical reaction. The total reduction time is expressed by Eq. (6) [35], which is valid under the conditions of solid sphere being reacted with gas phase and the effect of external diffusion of gas being negligible. So the reaction rate could be controlled by the interfacial chemical reaction and the internal diffusion of reactant and product gas species through solid product layer.

$$t = \frac{r_0^2 \rho_0}{D_e(C_0 - C_q)}[1/2 - w/3 - (1-w)^{2/3}/2] +$$
$$+ \frac{r_0 \rho_0}{k(C_0 - C_q)}[1 - (1-w)^{1/3}] \qquad ...(6)$$

Where t is reduction time (s), C_0 and C_q are reduction gas concentration at granule surface and in equilibrium, respectively (mol/m^3), k is reaction rate constant (m/s), D_e is effective diffusion coefficient (m^2/s), r_0 is characteristic initial radius of pellet (m), ρ_0 is initial oxygen concentration in the pellet (mol/m^3), and w is fraction reaction (same as w in Eq. (1)).

Considering that the reduction of TTM concentrate is a multi-step complex process with no single reaction that continues throughout reduction process, C_q is difficult to be calculated exactly which is related to the equilibrium constant determined by the dominant reaction.

Define $\frac{r_0}{D_e}\frac{r_0\rho_0}{(C_0 - C_q)} = \frac{1}{D_e'}$ and $\frac{1}{k}\frac{r_0\rho_0}{(C_0 - C_q)} = \frac{1}{k'}$, where D_e',

Table 2. *Compositions of titanomagnetite concentrate particles during the reduction by 50 vol% CO-Ar mixtures (EDS analysis, points on Fig. 8, at.%)*

Point No.	O	Fe	Ti	Mg	Si	Ca	Al	Mn
1	51.16	20.05	3.62	6.57	0.12	0	17.27	0.14
2	50.85	33.65	4.74	2.05	0.16	0.05	7.35	0.17
3	1.72	94.53	0.86	0.01	0.09	0.03	0.07	2.58
4	61.48	6.08	0.14	7.17	0.12	0.03	24.76	0.23
5	53.6	43.42	0.53	0.87	0.06	0	0.12	1.39
6	58.4	31.13	7.44	0.68	0.09	0.06	1.17	1.03
7	1.91	94.25	0.96	0.06	0.08	0.05	0.1	2.35
8	60.55	16.58	6.96	4.56	5.43	0.12	5.17	0.63
9	42.75	36.76	11.28	2.16	0.23	0.08	5.13	1.6

is apparent effective diffusion coefficient and k' is apparent reaction rate constant. In the following kinetics analysis, both D_e and k appear in the first power form, so the using of D_e' and k' has no affect on relative comparison.

By plotting the linear regression relationship between $\dfrac{t}{1-(1-w)^{1/3}}$ and $\dfrac{[1/2-w/3-(1-w)^{2/3}/2]}{[1-(1-w)^{1/3}]}$, D_e' and k' can be obtained from slope and intercept, respectively. The calculated values of D_e' and k' at different temperatures are list in Table 3.

Table 3. *The calculated values of D_e' and k' at different temperatures*

	1123 K	1173 K	1223 K	1273 K	1323 K
D_e'	1.87×10^{-5}	1.96×10^{-5}	2.11×10^{-5}	2.37×10^{-5}	2.91×10^{-5}
k'	6.40×10^{-5}	7.99×10^{-5}	1.05×10^{-4}	1.42×10^{-4}	1.91×10^{-4}

It can be seen from Table 3 that both D_e' and k' values increase with temperature increasing. The value of k' at 1323 K is 2.98 times than it 1123 K, and that of D_e' is 1.56 times, which means that temperature has stronger influence on interfacial chemical reaction. And the resistances of internal diffusion (R_i) and interfacial chemical reaction (R_c) can be calculated as follow formulas[36]:

$$R_i = \frac{r_0}{D_e}(\frac{r_0}{r_i}-1) \qquad \text{...(7)}$$

$$R_c = \frac{1}{k}\frac{r_0^2}{r_i^2} \qquad \text{...(8)}$$

Where r_i is the radius of unreacted core (m) in the reduction process. Assuming densities of solid reactant and its product are approximately the same, r_i can be expressed by w as bellow [36]:

$$r_i = r_0(1-w)^{1/3} \qquad \text{...(9)}$$

So, by some mathematical rearrangements, the apparent resistance of internal diffusion R_c' and interfacial chemical reaction R_i' at different temperatures can be calculated using D_e' and k', as shown in Figs. 9 and 10. Due to the grown of reaction layer and the decrease of reaction interface area with reduction processing, both R_c' and R_i' increases gradually and this is more significant at the late stage of reduction. And the difference of resistances at the same reduction degree also enlarged with reduction processing. At the same reduction degree, the resistances are lowered by temperature rising. This is because interfacial chemical reaction and internal diffusion are accelerated at high temperature.

For further investigation of the reaction rate controlling step, the relative resistances of internal diffusion ($R_i'\% = R_i'/R_\Sigma'$) and interfacial chemical reaction ($R_c'\% = R_c'/R_\Sigma'$) were calculated with $R_\Sigma' = R_i' + R_c'$. As seen in Fig. 11, in the experimental temperature range,
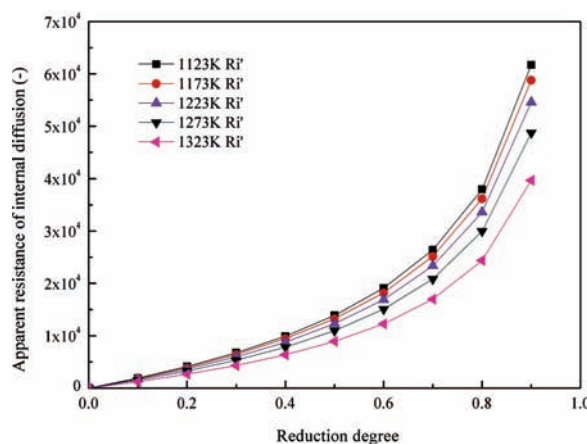

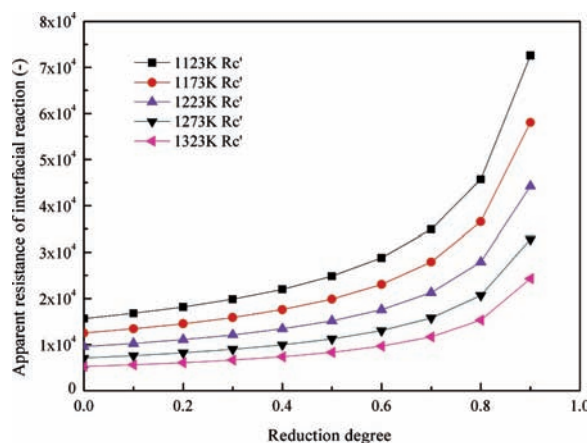**Figure 9.** *The apparent resistance of internal diffusion at different temperatures*

Figure 10. *The apparent resistance of interfacial chemical reaction at different temperatures*

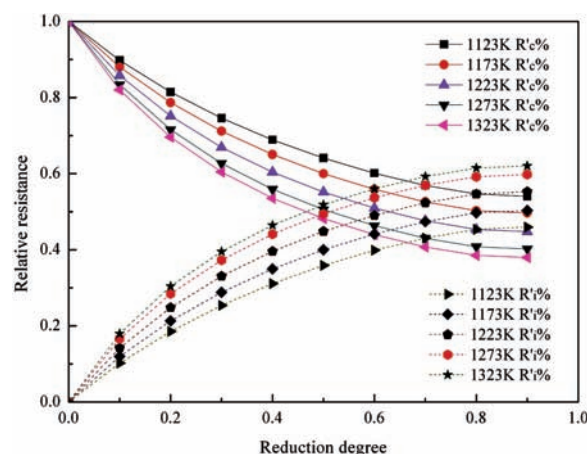$R_c'\%$ and $R_i'\%$ approach each other gradually with reduction processing. The relative resistance of

Figure 11. *The relative resistances for reduction of titanomagnetite concentrate by 50 vol% CO-Ar mixtures from 1123 K to 1323 K*
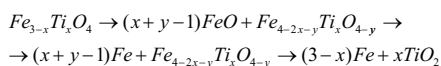
interfacial chemical reaction is dominant at the beginning of reduction meaning that reduction is controlled by interfacial chemical reaction at early stage of the reaction. And it is also can be seen that, the higher the temperature, the smaller the different of value between $R_c'\%$ and $R_i'\%$. At 1123 K, $R_c'\%$ is larger than $R_i'\%$ in the whole reduction process. But starting from 1173 K, there is an intersection appears and the intersection moves to the beginning of reduction gradually with temperature rising, which indicates that the controlling step of reduction turns from interfacial chemical reaction to the internal diffusion and the internal diffusion controlling range is expanded by temperature rising.

4. Conclusions

Generally, the reduction of TTM concentrate with CO-Ar gas mixtures proceeded topochemically. Increase of temperature and CO content was beneficial to the reduction of ilmenite concentrate. The low reduction rate is owing to the low iron oxides content and high impurities such as magnesium oxide in TTM concentrate which hindered reduction of Fe^{2+}.

Due to the microscopic non-homogeneity of TTM particle, the structure of reduced TTM concentrate is rough and porous, and the reduced iron phase accumulates on the in-situ unreduced reticular slag phase. The reduced slag distributes in the reduced iron dispersedly.

During the reduction, TTM concentrate was reduced to iron and iron-titanium oxides or titanium oxides, depending on the reduction temperature and time. The reduction path at temperatures above 1123 K is suggested as follow:

$$Fe_{3-x}Ti_xO_4 \rightarrow (x+y-1)FeO + Fe_{4-2x-y}Ti_xO_{4-y} \rightarrow$$
$$\rightarrow (x+y-1)Fe + Fe_{4-2x-y}Ti_xO_{4-y} \rightarrow (3-x)Fe + xTiO_2$$

(0<y<4-2x, x=0.27±0.02)

The resistances of internal diffusion and interfacial chemical reaction increase with reduction processing and decrease with temperature rising, which is more significant at the late stage of reduction. At early stage of the reaction, the reduction is controlled by interfacial chemical reaction and then the controlling step of reduction turns to the internal diffusion as the reaction processing. And the internal diffusion controlling range is expanded by temperature rising.

Acknowledgements

References

[1] Y.M. Wang, Z.F. Yuan, Z.C. Guo, Q.Q. Tan, Z.Y. Li, W.Z. Jiang, Nonferr. Metal. Soc., 18 (4) (2008) 962.

[2] W.S. Zhang, Z.W. Zhu, C.Y. Cheng, Hydrometallurgy, 108 (2011) 177.

[3] H.Y. Sun, J.S. Wang, X.J. Dong, Q.G. Xue, Metal. Int., 17 (7) (2012) 49.

[4] E. Park, O. Ostrovski, ISIJ Int., 43 (9) (2003) 1316.

[5] U.S. Geological Survey, USGS Mineral Commodity Summaries 2011, Unit State Geologic, Washington, 2011.

[6] S.L. Yang, J.F. Sheng, Technology of pig iron and titanium slag smelting. Metallurgy Industry Press, Beijing, 2006.

[7] L. Zhang, L.N. Zhang, M.Y. Wang, Miner. Eng., 20 (2007) 684.

[8] L.S. Li, Z.T. Sui, Acta Phys. Chim. Sin., 17 (2011) 845.

[9] P.C. Pistorius, C. Coetzee, Metall. Mater. Trans. B, 34 B (2003) 581.

[10] N. El-Hazek, T.A. Lasheen, R. El-Sheikh, S.A. Zaki, Hydrometallurgy, 87 (1-2) (2007) 45.

[11] A. Andrew, Y. Li, G.Q. Zhang, O. Oleg, Int. J. Miner. Process., 100 (3-4) (2011) 166.

[12] C.S. Kucukkaragoz, R.H. Eric, Miner. Eng., 19 (2006) 334.

[13] T. E. Dancy, Scand. J. Metall., 22 (3) (1993) 100.

[14] A.D. Pelton, C.W. Bale, Direct Reduced Iron: technology and economics of production and use, Iron & Steel Society,Warrendale, 1999.

[15] P. L. Vijay, R. Venugopalan, D. Sathiyamoorthy, Metall. Mater. Trans. B, 27 (5) (1996) 731.

[16] E. Park, O. Ostrovski, ISIJ Int., 43 (9) (2003) 1316.

[17] Y.M. Wang, Z.F. Yuan, H. Matsuura, F. Tsukihashi, ISIJ Int., 49 (2) (2009) 164.

[18] B. B. Agrawal, K. Prasad, H. S. Ray, ISIJ Int., 30 (8) (1990) 997.

[19] G. B. Sadykhov, L. O. Naumova, V. A. Rezinchenko, Russ. Metall., (1992), 15.

[20] G. D. McAdam, Ironmaking Steelmaking, 1 (1974) 138.

[21] E. Park, S. B. Lee, O. Ostrovski, D. J. Min, C. H. Rhee, ISIJ Int., 44 (1) (2004) 214.

[22] D.G. Jones, Trans. Inst. Min. Metall., 83 (808) C (1974) C1.

[23] R. Merk, C.A. Pickles, Can. I. Min. Metall., 27 (3) (1988) 179.

[24] K.G. Suresh, V. Rajakumar, P. Grieveson, Metall. Mater. Trans. B, 1987, 18 B (1987) 713.

[25] K.G. Suresh, V. Rajakumar, P. Grieveson, Metall. Mater. Trans. B, 18 B (1989) 735.

[26] N. Towhidi, J. Szekely, Metall. Trans. B, 14 B (1983) 359.

[27] S.Q. Deng, C.R. Che, L.J. Yan, Iron and steel, 28 (12) (1993) 12.

[28] E. Park, O. Ostrovski, ISIJ Int., 44(6) (2004) 990.

[29] S. Itoh, O. Inoue, T, Mater. Trans. JIM, 39(3) (1998) 391.

[30] O. Inoue, S. Itoh, T. Azakami, J. Jpn. I. Met., 60 (9) (1996) 834.

[31] S. Akimoto, J. Geomag. Geoelect., 6 (1) (1954) 1.

[32] H.Y. Sun, J.S. Wang, X.J. Dong, Q.G. Xue, Adv. Mater. Res., 402 (2012) 90.

[33] H. W. Kang, W. S. Chung, T. Murayama, Y. Ono, ISIJ Int., 38 (4) (1998) 324.

[34] A. Habermann, F. Winter, H. Hofbauer, J. Zirngast, J. L. Schenk, ISIJ Int., 40 (10) (2000) 935.

[35] O. Levenspiel, Chemical Reaction Engineering (2nd edn.), Wiley, New York, 1972.

[36] H.J. Guo, Physical Chemistry of Metallurgy (2nd edn.), Metallurgy Industry Press, Beijing, 2006.